Available online at www.sciencedirect.com
ScienceDirect
Ceramics International 34 (2008) 1661–1666
CERAMICS INTERNATIONAL
www.elsevier.com/locate/ceramint

Characterization of nanocrystalline manganese oxide powder prepared by inert gas condensation

Chin-Yi Chen [a], Chung-Kwei Lin [a,*], Ming-Hsiu Tsai [a], Chien-Yie Tsay [a], Pee-Yew Lee [b], Giin-Shan Chen [a]

[a] *Department of Materials Science and Engineering, Feng Chia University, Taichung 40724, Taiwan, ROC*
[b] *Institute of Materials Engineering, National Taiwan Ocean University, Keelung 20224, Taiwan, ROC*

Received 16 November 2006; received in revised form 27 April 2007; accepted 15 May 2007
Available online 12 August 2007

Abstract

Nanocrystalline manganese oxide powders were synthesized by an inert gas condensation technique. The manganese oxide powders, prepared from vaporized metallic manganese in a helium pressure of 10 mbar, then oxidized under the oxygen pressures of 50 and 100 mbar, exhibited a mixture of β-Mn, MnO and Mn_3O_4 phases. X-ray diffractometry (XRD) analysis identified the predominant oxide formation of the as-prepared powder to be the phase of MnO. *In situ* synchrotron XRD and differential scanning calorimetry (DSC) data showed that synthesized manganese powder converts from β-Mn to MnO in the temperature range of 150–250 °C and subsequently converts to Mn_3O_4 above 250 °C. Transmission electron microscopy examinations confirmed that oxidation starts from the surface of the condensed β-Mn particles. Detailed valance variations of manganese of the resulting powders were investigated by synchrotron X-ray absorption spectroscopy techniques.

Keywords: B. X-ray methods; C. Thermal properties; Gas phase reaction; Manganese oxide; *In situ* synchrotron X-ray diffractometry

1. Introduction

Nanoparticles have attracted considerable interest in various physical and chemical fields since their fundamental properties are found relatively different from those of their corresponding bulk state. Accordingly, a number of methods have been developed for the preparation of metal/oxide particles, such as gas condensation method [1–6] and sol–gel process [7–9]. In gas condensation, the particle formation and solidification occur when undercooled metal droplets with a ''liquid-like'' amorphous state which is generated from supersaturated metal vapor at a moderately rapid undercooling rate. This technique is thus commonly used to synthesize nanosized and metastable phased materials [6].

Manganese oxides, where the manganese can exhibit in many different valence states, are promising supercapacitor materials due to the low cost of raw materials and the fact that manganese is considered more environmentally friendly than other noble metal oxides [10–12]. In previous studies, Dimesso et al. [3] have demonstrated that manganese oxides can be prepared by an inert gas condensation technique by annealing in air and oxygen at various temperatures for different times. The predominant phase of MnO and Mn_3O_4 are obtained after annealing at a temperature of 400 °C in air. The particle size of the nanocrystalline manganese is found to be increases with the increasing time. In addition, the growing interest in supercapacitors has been stimulated by their potential application as electric storage devices operating in parallel with the battery in an electric vehicle to transiently provide high power [13,14]. Supercapacitors fill the gap between batteries and conventional capacitors in terms of their specific energy and specific power.

In the present work, manganese oxide powders were prepared by an inert gas condensation technique. Various pressures of oxygen were filled into the chamber where manganese raw material was heated and oxidized after the condensation of manganese powder. The prepared nanocrystalline manganese oxides were characterized by conventional X-ray diffractometry (XRD), transmission electron microscopy (TEM), differential scanning calorimetry (DSC), *in situ* synchrotron X-ray diffractometry and X-ray absorption

* Corresponding author. Tel.: +886 4 24517250x5309; fax: +886 4 24510014.
E-mail address: cklin@fcu.edu.tw (C.-K. Lin).

0272-8842/$34.00
doi:10.1016/j.ceramint.2007.05.013

spectroscopy. The characterization results provide invaluable information to further processing and performance of these manganese oxide-based supercapacitors.

2. Experimental methods

2.1. Manganese oxide powder preparation

The manganese oxide powder was prepared using an inert gas condensation technique. The schematic representation of the experimental setup is shown in Fig. 1. The system consisted of (a) a vacuum chamber with a vacuum system, (b) a heating power supply with a temperature control system, (c) an atmospheric control system to obtain the product powder with a desired composition, and (d) cooling system with a liquid nitrogen piped cold trap. The vacuum chamber includes a tungsten boat for melting the bulk manganese, a vacuum pumping system, a vacuum gauge, and a cold trap for powder condensation. The manganese metal was placed in the tungsten crucible in the vacuum chamber under a helium atmosphere. The pressure of the helium gas was maintained at 10 mbar before the evaporation of manganese. The tungsten crucible is heated by a dc-voltage provided resistance heating source. The helium gas decreases the kinetics of metal atoms by colliding the particles with each other during the condensation, controlling the growth and/or coalescence of the particles [15]. The manganese metal was then thermally evaporated into metallic vapor, condensing rapidly onto the cold trap to form fine particles. The cold trap is cooled with piped liquid nitrogen. After condensing the manganese, oxygen gas with respective pressures of 50 and 100 mbar was then refilled to react with the metallic manganese to form manganese oxides. The separation between the melted metal and the cold trap was optimized to control the nucleation-growth process for obtaining fine powders with appropriate particle sizes.

2.2. Characterization of manganese oxide powder

The phase identification of the product powders was performed by XRD (SRA M18XHF, MAC. Science Co., Japan) with a Cu Kα radiation (λ = 1.54184 Å) in the 2θ range 30–90° at a scanning rate of 6° 2θ/min. The respective operation electrical voltage and current are 50 kV and 200 mA. The morphology of the resulting powders was observed using transmission electron microscopy (Model 800, HITACHI Co., Tokyo, Japan). The thermal behavior of the prepared powders was determined by a differential scanning calorimetry (SDT-2960, Simultaneous DSC-TGA, TA Instrument) under gaseous argon with a flow rate of 25 ml/min for removal of product gases.

In situ synchrotron XRD identifications were performed with increasing the heating temperature at the National Synchrotron Radiation Research Center (NSRRC), Hsinchu, Taiwan; with an intense photon flux from the Wiggler-A beamline using a constant wavelength of 1.3271 Å. The X-ray absorption spectroscopy (XAS) was also performed at the NSRRC; with a photon flux from the Wiggler-C beamline. The Wiggler-C beam-line was optimized for X-ray photon energy in the 0.8–15 KeV range (the K-edge of Mn is at 6.54 KeV) for the transmission mode X-ray absorption near-edge structure (XANES) and extended X-ray absorption fine structure (EXAFS) measurements. The XANES was performed by measuring the Mn K-edge absorption spectra, determining the valence changes of manganese atoms. The Fourier transformation of the EXAFS spectra obtained from the individual shells of atoms were also measured to estimate the Mn–Mn and Mn–O distances for comparison. A manganese foil was used to calibrate the photon energy before and after the EXAFS exams.

3. Results and discussion

The nanocrystalline manganese oxide powder was prepared from the vaporized manganese in a helium atmosphere, and then reacted with the introduced oxygen gas at the respective oxygen pressure of 50 and 100 mbar. Fig. 2 shows the X-ray diffraction patterns of the nanocrystalline manganese oxide powders under different oxygen partial pressures. The as-deposited powders were identified as a mixture of β-Mn (majority), MnO, and Mn_3O_4 phases. The presence of impure

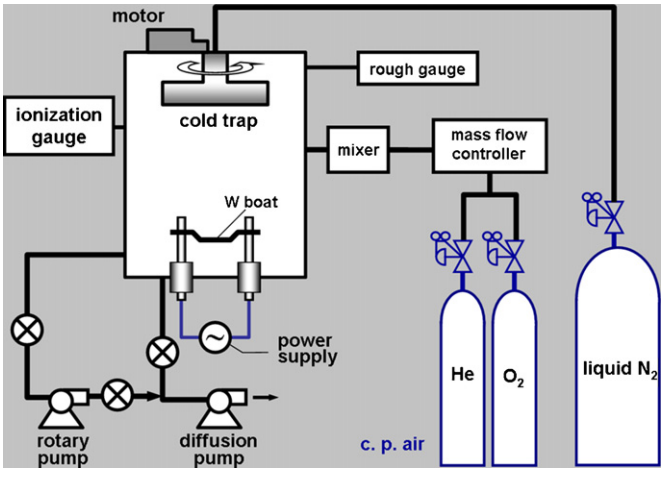

Fig. 1. The schematic representation of gas condensation setup.

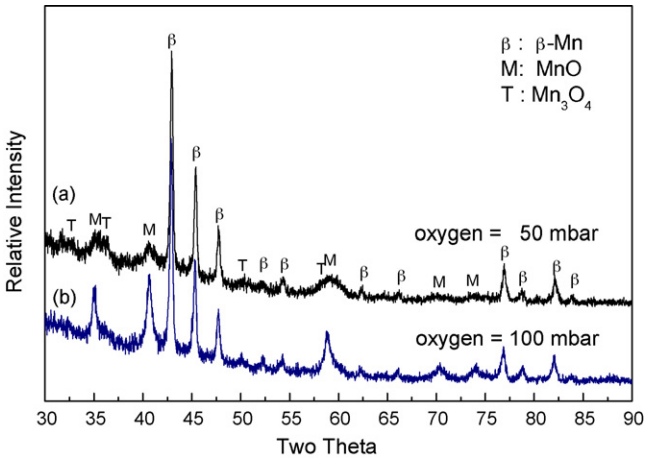

Fig. 2. X-ray diffraction patterns of the as-prepared powders under different oxygen partial pressure.

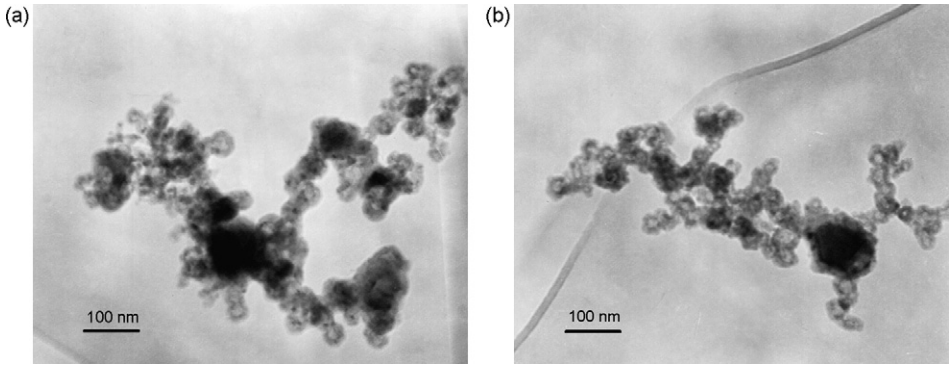

Fig. 3. TEM micrographs of the as-prepared powders under oxygen partial pressures of (a) 50 mbar and (b) 100 mbar.

gases such as oxygen, nitrogen, and water vapors may obstruct the metal atoms to increase the condensation time from the vaporization source to the cold trap. It leads the manganese atoms to form larger particles or oxidize into MnO and/or Mn_3O_4. The predominant formation of oxides shown in Fig. 2 was identified as the phase of MnO. The relative intensity of MnO diffraction peaks increases with the increase of the oxygen partial pressure, whereas the relative intensity of Mn_3O_4 diffraction peaks shows no significant change in XRD data. Moreover, the relative intensity of diffraction peaks of β-Mn decreases with increasing the oxygen partial pressure due to the decrease of the amount of β-Mn, though the phase of β-Mn is still the majority.

Fig. 3 shows the TEM micrographs of the nanocrystalline manganese oxide powders under the oxygen partial pressures of 50 and 100 mbar. In both the micrographs, the dark particles are found to be the β-Mn with larger particle size, while the smaller particles with a chain-like morphology are believed to be the MnO and the Mn_3O_4. With increasing the oxygen pressure, β-Mn reacted with oxygen to result in the formation of Mn-oxides (MnO and Mn_3O_4). It implies that the amount of β-Mn deceases with the increase of oxygen pressure, whereas, the amount of Mn-oxides increases. The results show a good agreement with the increasing peaks of Mn-oxides in Fig. 2. The oxidation started on the surface of the β-Mn particles, leading the transparent oxide shell to be found on the β-Mn particles in the TEM micrographs. A comparison of Figs. 2 and 3, the oxide shell covered on the large β-Mn particles tended to prevent the further oxidation of the metallic manganese. The residual β-Mn thus retains in the core of the particles, exhibiting the major phase of β-Mn in all the product nanocrystalline manganese even after the treatment of oxygen atmosphere.

Due to the high surface energy of nanocrystalline particles as well as their unstable thermal properties, the DSC analysis was used for the determination of thermal behavior of as-prepared powders, as shown in Fig. 4. The DSC was carried out in the temperature range from room temperature to 500 °C at a heating rate of 5 °C/min under a gaseous argon flow for preventing oxidation of nanocrystalline manganese. It can be noticed that two exothermic peaks occur in the temperatures ranges of 150–250 °C and 300–350 °C. In the previous study, Berbenni and Marini [16] demonstrated the results from the non-nanoscale manganese particles that metal manganese (α-Mn or β-Mn) first transforms into MnO at ∼300 °C, and subsequently converts from MnO to Mn_3O_4 at ∼500 °C. A comparison with the DSC data, it can be found in Fig. 4 that the temperature of the phase transformation was reduced obviously due to the high surface area of the nanosize manganese particles. The nanocrystalline manganese underwent phase transitions in lower temperature ranges, indicating that the high surface energy of the nanosize particles may overcome easily the energy barrier of the transformation. The particle size thus influenced significantly the thermal behavior of the powders. From the data of DSC analysis in Fig. 4, the exothermic peak in the temperature range of 150–250 °C attributed to the conversion of β-Mn to MnO. Because the β-Mn particles were larger in size and covered with an oxide shell (Fig. 3(a)), the transformation of β-Mn to MnO exhibited a broadened peak due to the higher conversion energy. With increasing the oxygen pressure up to 100 mbar, the dashed line in Fig. 4, the thickness of the oxide shell on the β-Mn particles increased to result in the higher conversion energy. Moreover, the exothermic peak for the temperature range of 300–350 °C is believed to be the conversion of MnO to Mn_3O_4. Because the transformation of MnO to Mn_3O_4 resulted from the valence change of manganese, the exothermic reaction showed to be less significant than that of β-Mn to MnO.

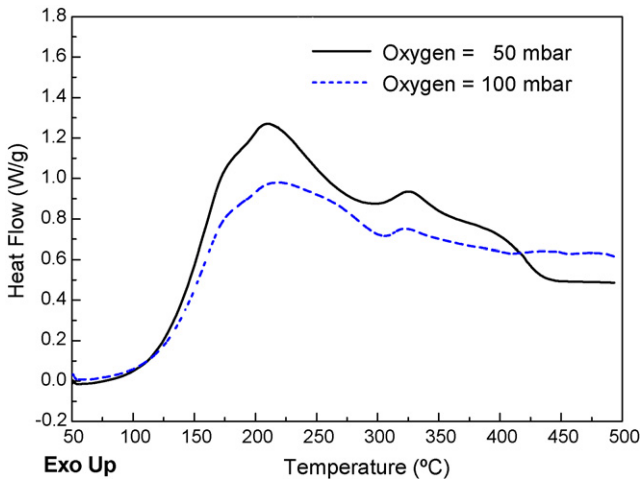

Fig. 4. DSC curves of the as-prepared powders under different oxygen partial pressure.

In order to investigate the phase evolutions of the as-prepared powders, *in situ* synchrotron X-ray diffractometry was carried out with the increasing temperature using a constant wavelength of 1.3271 Å. Figs. 5 and 6 show the *in situ* synchrotron XRD patterns of the nanocrystalline manganese under oxygen pressures of 50 and 100 mbar as a function of heating temperature. The β-Mn phase prepared under the oxygen pressure of 50 mbar is found, in Fig. 5, to transform into MnO at the early stage of the heating process. The relative intensity of β-Mn peaks decreased gradually with the increasing temperature, whereas that of MnO peaks increased. When the heating temperature was up to 300 °C, no obvious β-Mn peaks can be found, implying that the β-Mn converted into Mn-oxides completely. Similarly, the Fig. 6 reveals that the relative intensity of β-Mn peaks decreased with the increasing temperature as the powder was treated under the oxygen pressure of 100 mbar. Whereas, the MnO is found to exist in the as-prepared powder at room temperature; the relative intensity of the MnO peaks increased slightly from room temperature to 250 °C. Subsequently, the phase transition of MnO to Mn_3O_4 occurred when the temperature elevated to 300 °C. The Mn_3O_4 is thus expected to be a stable phase when the temperature higher than 300 °C. Comparison of the nanocrystalline manganese oxide powder treated in both the oxygen pressures, because the oxide shell covered on the β-Mn

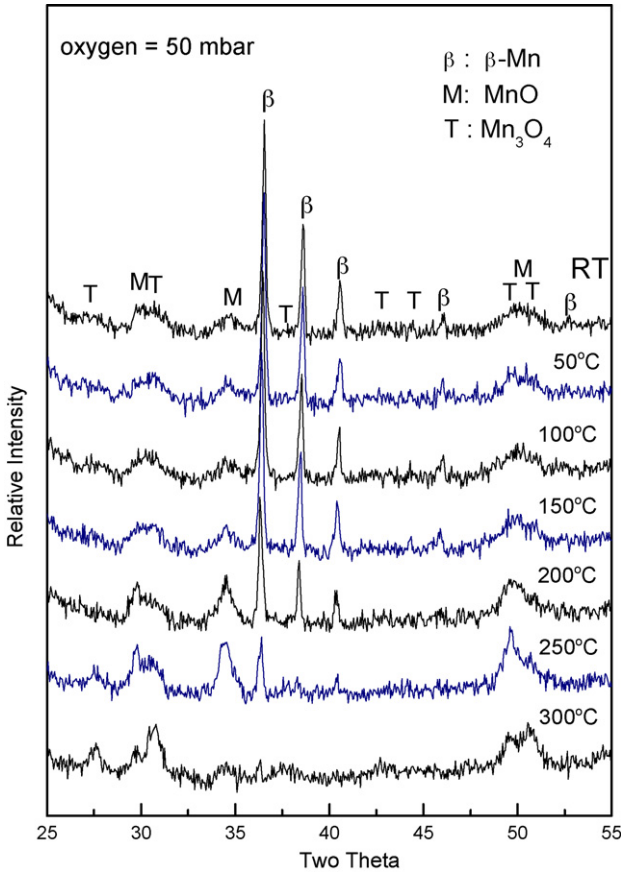

Fig. 5. *In situ* synchrotron X-ray diffraction patterns of the as-prepared powder under a oxygen pressure of 50 mbar as a function of heating temperature.

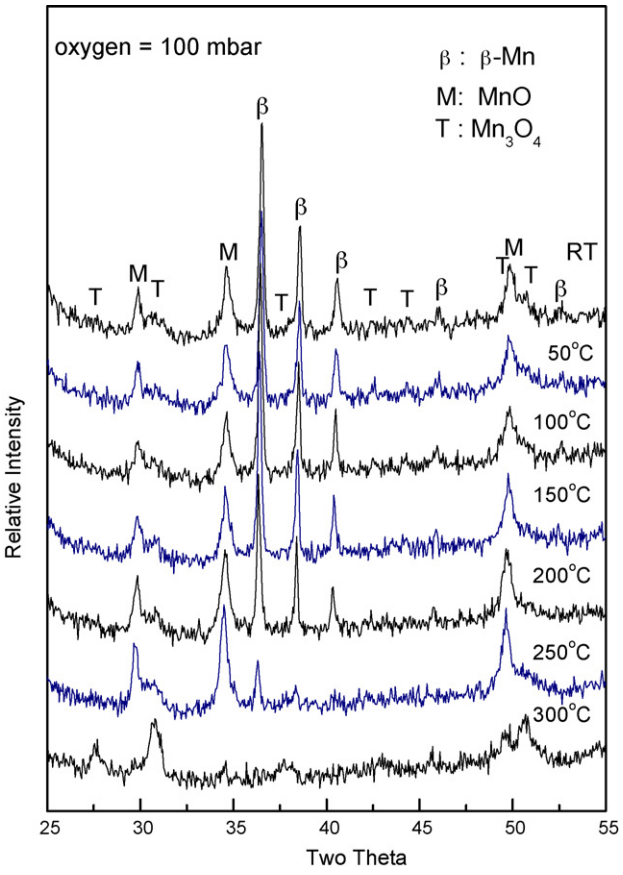

Fig. 6. *In situ* synchrotron X-ray diffraction patterns of the as-prepared powder under a oxygen pressure of 100 mbar as a function of heating temperature.

particles was relatively thin, a conversion of β-Mn to MnO occurred in the powder prepared under the oxygen pressure of 50 mbar in lower temperature range of 150–250 °C. However, when the manganese oxide powder is treated with 100 mbar oxygen, the thickness of the oxide shell covered on the β-Mn was increased, leading to the raise of conversion temperature in the range of 200–250 °C. It shows a good agreement with that of DSC analysis in Fig. 4. The results served to confirm that the Mn-oxides can be prepared from the heated manganese powder at a constant temperature without further oxygen treatment.

Comparison of the *in situ* XRD data and the DSC analysis, DSC curves show the reaction peaks within the temperature ranges of 150–250 °C for the formation of MnO, and 300–350 °C for the formation of Mn_3O_4. Though the MnO phase was present in the as-prepared powders which were treated in both the oxygen pressures of 50 mbar and 100 mbar, the intensity of MnO peaks relative to that of β-Mn peaks increased in the temperature range of 150–250 °C, implying the formation of MnO phase. It shows an agreement with the results of DSC analysis. Moreover, though the temperature range of 250–300 °C shown in the *in situ* XRD data did not satisfy the highest value for the formation of Mn_3O_4 shown in DSC data, the relative intensity of MnO to Mn_3O_4 decreased in such the temperature range, suggesting the conversion of MnO to Mn_3O_4. Therefore, the formation of Mn_3O_4 does not only

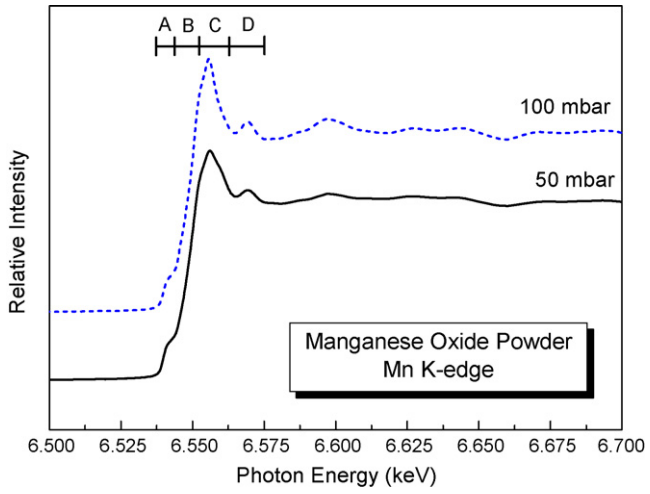

Fig. 7. Manganese K-edge absorption spectra for the as-prepared nanocrystalline manganese oxide powders under different oxygen partial pressure.

start above the temperature of 300 °C for the results of DSC analysis, but also generates above 250 °C for the evidence of *in situ* XRD identification.

Synchrotron X-ray absorption technique was carried out for the local structure (short range) identifications of manganese in nanocrystalline powders treated in various oxygen pressures. In the previous study [17–20], the energy of the main absorption edge was found to be increased when manganese valence increases, implying that the Mn valence structures with different energy regions can be distinguished in the Mn K-edge spectrum. Fig. 7 shows the X-ray absorption spectra for the as-prepared powders treated under various oxygen pressures. The prepared nanocrystalline manganese oxide powders were identified by XRD analyses to be the phases of β-Mn, MnO and Mn_3O_4. Because the respective Mn valences of β-Mn, MnO and Mn_3O_4 in the prepared powder are 0, +2 and +2.67, the X-ray absorption spectra are contributed by the manganese ions with the three different valences. Fig. 8 shows the one-order differential curves obtained from the XANES spectra in Fig. 7. In both the Figs. 7 and 8, four major regions, A, B, C and D, are labeled in these spectra due to their different features. The features of the XANES spectra found in this system are quite similar. These are assumed to result from the similar nature of the orbitals involved in these manganese structures. Such the effects caused by the atomic orbitals and electronic states of manganese can not offer significant energy shift in these XANES spectra; whereas, only influence the relative intensity caused by different absorption energy involved in the transitions between electronic states. Comparing the two differential XANES spectra for the nanocrystalline manganese oxide powders prepared in various oxygen pressures, Fig. 8, the differential peaks were found to be almost at the same energy, but showed small changes in intensities. In region A, the differential peak reveals a slight decrease in relative intensity when manganese oxide powder is synthesized in oxygen pressure of 100 mbar. The reduction is believed to result from the increase of coordination number which is caused by the insertion of oxygen ion between Mn atoms. Similarly, the differential peak at 6551 eV in region B reveals a significant increase when the oxygen pressure

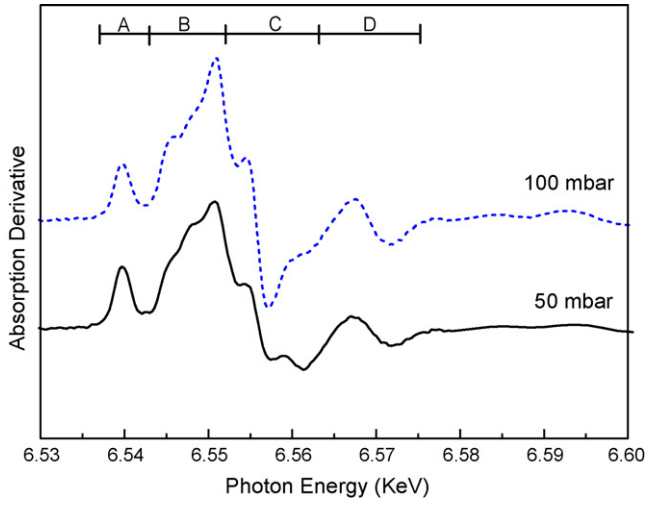

Fig. 8. One-order differential XANES spectra for the as-prepared nanocrystalline manganese oxide powders under different oxygen partial pressure.

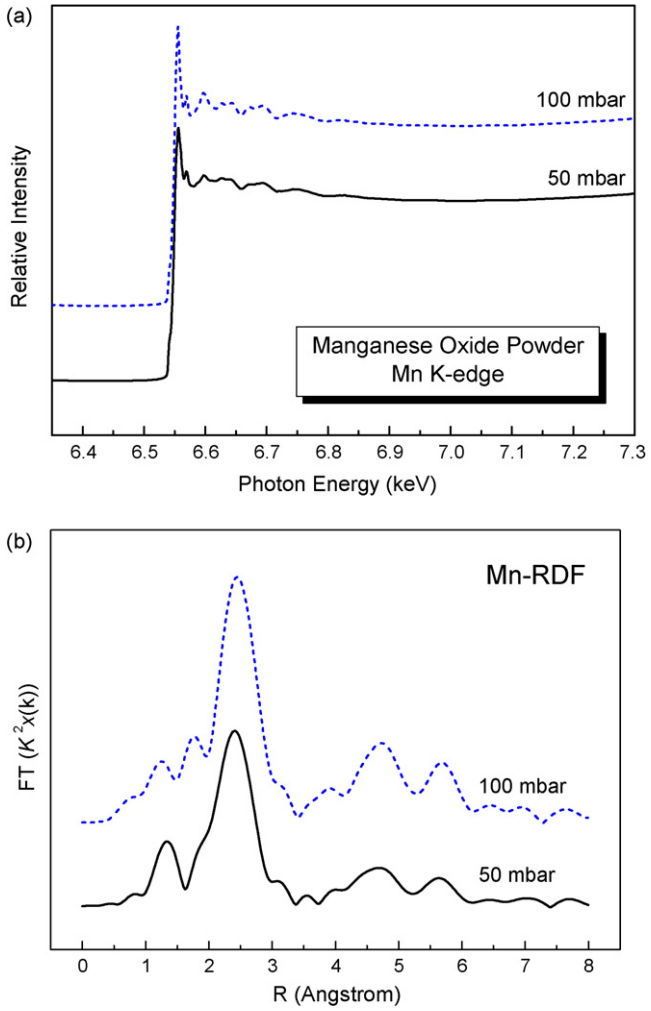

Fig. 9. (a) EXAFS spectra and (b) radial distribution functions for the as-prepared nanocrystalline manganese oxide powders under different oxygen partial pressures.

increases to 100 mbar. It generally results from the higher orbital symmetry in electronic structure of manganese as the Mn_3O_4 increases. In regions C and D, because the effect of the neighboring atom of Mn increased with the increasing oxygen pressure, the amplitude of the differential XANES spectra was thus enhanced.

The interatomic distance of the nanocrystalline manganese can be determined accurately by radial distribution function (RDF) which is obtained from Fourier transformation of EXAFS spectra. Fig. 9(a) shows the EXAFS spectra for the nanocrystalline manganese oxide powders under various oxygen partial pressure; and their RDF curves are obtained from the EXAFS spectra, as shown in Fig. 9(b). Though there was no significant change can be found in the EXAFS spectra in Fig. 9(a), whereas the first peak at 1.4 Å and the second peak at 1.9 Å shown in their RDF curves, Fig. 9(b), can attribute to the Mn–O bonding in manganese oxide powder. Because the oxidation of product powder mixture synthesized in 100 mbar oxygen pressure was more significant, the Mn–O peak at 1.9 Å enhanced by both the MnO and Mn_3O_4 structures showed higher amplitude than that of the resulting powder synthesized in 50 mbar oxygen pressure. Moreover, the peak at 2.5 and 3.1 Å were found to attribute to the Mn–Mn bonding, showing no significant changes at such the distances between the curves treated under the different oxygen partial pressures. In this system, the manganese oxides are not fully oxidized within the treatment of oxygen, resulting the weaker Mn–O peaks. The as-prepared powder thus exhibited a mixture of metallic manganese and manganese oxides.

4. Conclusions

The present study shows that the nanocrystalline manganese oxide powders are successfully prepared by the inert gas condensation technique. The manganese oxide powders, prepared in a He-atmosphere, exhibit a mixture of β-Mn, MnO and Mn_3O_4 phases after the treatment of oxygen. The predominant oxide formation of the mixture is identified to be the phase of MnO using XRD technique. Moreover, *in situ* synchrotron XRD and DSC data reveal that the as-prepared manganese powder converts from β-Mn to MnO in the lower temperature range of 150–250 °C and converts to Mn_3O_4 above 250 °C. With increasing the oxygen pressure, however, the formation of the oxide shell on the β-Mn increases slightly the transition temperature of β-Mn to MnO. Transmission electron microscopy examinations confirm that oxidation starts on the surfaces of the condensed β-Mn particles. By analyzing the detailed valance variations of manganese, synchrotron X-ray absorption spectroscopy techniques shows that the oxidation of resulting product manganese powders is increased with the increase of oxygen pressure.

Acknowledgements

The financial support of this work by the National Science Council of Republic of China under contract no. NSC94-2216-E-035-008 is gratefully acknowledged. The authors also thank the entire staff at NSRRC (Hsinchu, Taiwan, ROC) for the expert assistance.

References

[1] H.-M. Lin, C.-Y. Tung, Y.D. Yao, Y. Hwu, W.-L. Tsai, S.-J. Tzeng, C.-K. Lin, P.-Y. Lee, Magnetic and structural properties of nanophase Ag_xFe_{1-x} solid solution particles, Nanostruct. Mater. 10 (1998) 457–464.
[2] H.-M. Lin, C.-H. Keng, C.-Y. Tung, Gas-sensing properties of nanocrystalline TiO_2, Nanostruct. Mater. 9 (1997) 747–750.
[3] L. Dimesso, L. Heider, H. Hahn, Synthesis of nanocrystalline Mn-oxides by gas condensation, Solid State Ionics 123 (1999) 39–46.
[4] A. Tschope, D. Schaadt, R. Birringer, J.Y. Ying, Catalytic properties of nanostructured metal oxides synthesized by inert gas condensation, Nanostruct. Mater. 9 (1997) 423–432.
[5] C.-Y. Wu, H.-M. Lin, H.-F. Lin, M.-F. Tai, C.-R. Wang, C.-K. Lin, P.Y. Lee, Preparation and characterization of nanocrystalline Nb_3Al alloy, Scripta Mater. 44 (2001) 1967–1971.
[6] W. Krauss, R. Birringer, Metastable phases synthesized by inert-gas-condensation, Nanostruct. Mater. 9 (1997) 109–112.
[7] M. Sugantha, P.A. Ramakrishnan, A.M. Hermann, C.P. Warmsingh, D.S. Ginley, Nanostructured MnO_2 for Li batteries, Int. J. Hydrogen Energy 28 (2003) 597–600.
[8] O. Harizanov, T. Ivanova, A. Harizanova, Study of sol–gel TiO_2 and TiO_2–MnO obtained from a peptized solution, Mater. Lett. 49 (2001) 165–171.
[9] N.I. Kovtyukhova, E.V. Buzaneva, C.C. Waraksa, T.E. Mallouk, Ultrathin nanoparticle ZnS and ZnS: Mn films: surface sol–gel synthesis, morphology, photophysical properties, Mater. Sci. Eng. B 69–70 (2000) 411–417.
[10] J.N. Broughton, M.J. Brett, Investigation of thin sputtered Mn films for electrochemical capacitors, Electrochim. Acta 49 (2004) 4439–4446.
[11] B. Djurfors, J.N. Broughton, M.J. Brett, D.G. Ivey, Microstructural characterization of porous manganese thin films for electrochemical supercapacitor applications, J. Mater. Sci. 38 (2003) 4817–4830.
[12] Y.-S. Chen, C.-C. Hu, Y.-T. Wu, Capacitive and textural characteristics of manganese oxide prepared by anodic deposition: effects of manganese precursors and oxide thickness, J. Solid State Eletrochem. 8 (2004) 467–473.
[13] B.E. Conway, Transition from ‘‘Supercapacitor’’ to ‘‘Battery’’ behavior in electrochemical energy storage, J. Electrochem. Soc. 138 (1991) 1539–1547.
[14] S. Sarangapani, B.V. Tilak, C.P. Chen, Materials for electrochemical capacitors. Theoretical and experimental constraints, J. Electrochem. Soc. 143 (1996) 3791–3800.
[15] K. Kimoto, Y. Kamiya, M. Nonoyama, R. Uyeda, An electron microscope study on fine metal particles prepared by evaporation in argon gas, Jpn. J. Appl. Phys. 2 (1963) 702–713.
[16] V. Berbenni, A. Marini, Thermoanalytical (TGA-DSC) and high temperature X-ray diffraction (HT-XRD) study of the thermal decomposition processes in Li_2CO_3–MnO mixtures, J. Anal. Appl. Pyrol. 64 (2002) 43–58.
[17] W.E. O’Grady, K.I. Pandya, K.E. Swider, D.A. Corrigan, *In situ* X-ray absorption near-edge structure evidence for quadrivalent nickel in nickel battery electrodes, J. Electrochem. Soc. 143 (1996) 1613–1616.
[18] B. Brendebach, F. Reinauer, N. Zotov, M. Funke, R. Glaum, J. Hormes, H. Modrow, X-ray absorption near edge structure (XANES) investigation of MnO_y-doped sodium metaphosphate glasses and crystalline reference materials, J. Non-Cryst. Solids 351 (2005) 1072–1076.
[19] F. Bridges, C.H. Booth, G.H. Kwei, J.J. Neumeier, G.A. Sawatzky, Temperature dependent changes of the Mn 3d and 4p bands near T_c in colossal magnetoresistance systems: XANES study of $La_{1-x}Ca_xMnO_3$, Phys. Rev. B 61 (2000) 9237–9240.
[20] M. Belli, A. Scafati, A. Bianconi, S. Mobilio, L. Palladino, A. Reale, E. Burattini, X-ray absorption near edge structures (XANES) in simple and complex Mn compounds, Solid State Commun. 35 (1980) 355–361, 4.